Mössbauer and magnetization studies of Fe_3BO_5

2002 J. Phys.: Condens. Matter 14 3303

(http://iopscience.iop.org/0953-8984/14/12/317)

INSTITUTE OF PHYSICS PUBLISHING JOURNAL OF PHYSICS: CONDENSED MATTER

J. Phys.: Condens. Matter **14** (2002) 3303–3320 PII: S0953-8984(02)27069-1

Mössbauer and magnetization studies of Fe_3BO_5

A P Douvalis[1,3], A Moukarika[1], T Bakas[1], G Kallias[2] and V Papaefthymiou[1,4]

[1] Physics Department, University of Ioannina, PO Box 1186, 45 110 Ioannina, Greece
[2] Institute of Materials Science, National Centre for Scientific Research 'Demokritos', 153 10 Athens, Greece

Received 23 July 2001, in final form 8 February 2002
Published 15 March 2002
Online at stacks.iop.org/JPhysCM/14/3303

Abstract

We report on magnetometry, resistivity and Mössbauer spectroscopy measurements on single-phase Fe_3BO_5 in a wide temperature range from 4.2 to 620 K. Magnetically split Mössbauer spectra were observed below $T_N = 114$ K, although a proportion of the Fe^{2+} ions in the basal plane (crystallographic site Fe1) remain paramagnetic down to the ferrimagnetic transition at $T_w = 74$ K. This unusual magnetic behaviour known as 'idle-spin behaviour' can be explained by the competitive magnetic interactions with its neighbouring ordered ions and should be related to the topology of the octahedral Fe1 sites in the crystal structure of Fe_3BO_5. The behaviour change recorded in the dc magnetization and Mössbauer data indicates that the magnetic structure of Fe_3BO_5 should change at 74 K, where the spin frustration gradually ceases to exist. Electron delocalization in the Fe3–Fe2–Fe3 triads between pairs of Fe^{2+} and Fe^{3+} ions was observed at all temperatures between 4.2 and 180 K and coexists with localized ferric and ferrous (Fe1 and Fe4 crystallographic sites) states. Above 180 K the delocalization in the Fe3–Fe2–Fe3 triads includes the rest of the Fe^{3+} ions and some evidence can be seen in the resistivity data as well.

1. Introduction

The iron oxyborate Fe_3BO_5 is a mixed-valence iron oxide with very interesting electronic and magnetic properties [1–5] which belongs to the family of ludwigites with chemical formula $M_2M'BO_5$, where M and M′ are divalent and trivalent 3d metal ions, respectively. It is one of the homometallic members of this family, and it occurs naturally as the mineral vonsenite.

Crystal structure studies of Fe_3BO_5 [1, 2, 6, 7] have shown that this phase crystallizes in the orthorhombic space group $Pbam$. The Fe ions occupy the four crystallographically

[3] Present address: Physics Department, Trinity College, Dublin 2, Republic of Ireland.
[4] Author to whom any correspondence should be addressed.

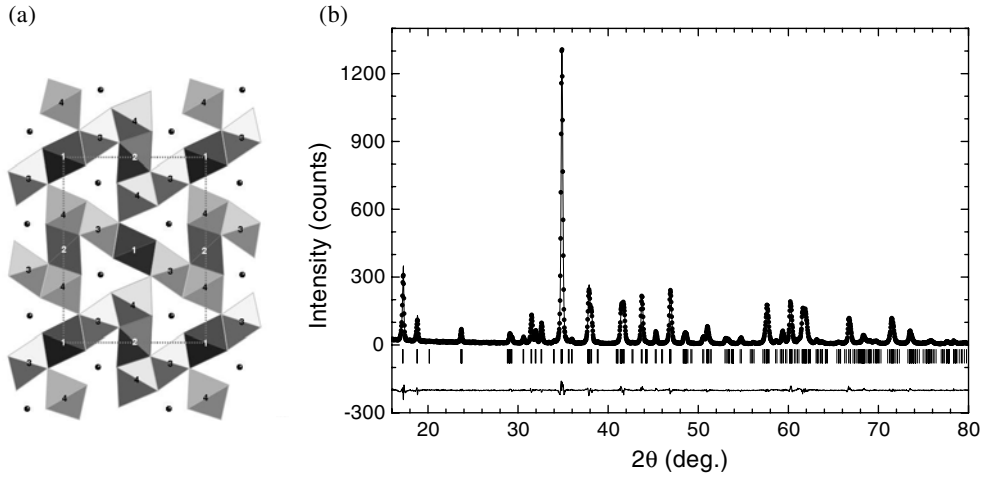

Figure 1. (*a*) The structure of Fe_3BO_5 at RT projected along the *c*-axis. The numbers 1, 2, 3 and 4 denote the octahedral iron sites Fe1, Fe2, Fe3 and Fe4, respectively. The black circles denote the B ions and the dashed line indicates the *a*- and *b*-axes of the unit cell. (*b*) The Rietveld refinement pattern for Fe_3BO_5 powder x-ray diffraction data at RT. The observed intensities are shown by filled symbols and the calculated ones by the solid curves. The positions of the Bragg reflections are shown by the small vertical lines below the pattern. The line at the bottom indicates the intensity difference between the experimental and refined patterns.

independent octahedral sites Fe1, Fe2, Fe3 and Fe4 [1, 2, 4], corresponding to 2a, 2d, 4h and 4g in Wyckoff's notation. Mössbauer and XRD studies [1–7] (at room temperature (RT)) are consistent with the presence of two pairs of physically distinct iron ions. Fe1 and Fe4 are divalent and located in the $z = 0$ plane. Fe2 and Fe3 are in intermediate oxidation states due to electron-delocalization phenomena and are located in the $z = 1/2$ plane. The structure in a (001) polyhedral view can be viewed as comprising edge- and corner-sharing chains of FeO_6 octahedra, as shown in figure 1(*a*) [2,4]. This gives rise to a 3D assembly in the form of zigzag walls. Several studies of the magnetic properties [3–5] have shown that the system undergoes an antiferromagnetic transition at $T_N = 114$ K which involves essentially only a proportion of the ferrous and all the ferric and intermediate-valence iron ions, then becomes a weak ferromagnet around 75 K (where all Fe ions are magnetically ordered) and below 40 K the ferrimagnetic state disappears. Charge-delocalization phenomena were observed above 114 K [3–5]. A rather similar behaviour in the magnetic and electronic properties was observed in a closely related compound, the warwickite Fe_2BO_4 [2, 8, 9], which is a mixed-valence and monoclinic compound below RT with two metal-ion sites.

Previous Mössbauer investigations of this synthetic oxide and of the corresponding mineral vonsenite [1, 3, 4, 10] have dealt essentially with the temperature range above T_N. In this work we decided to extend these studies down to a temperature of 4.2 K using also dc magnetization and resistivity measurements. Our aim is to give a consistent account of the complicated behaviour presented below the antiferromagnetic ordering temperature.

2. Experimental procedures

Polycrystalline Fe_3BO_5 was prepared by solid-state reaction of a stoichiometric mixture of $FeBO_3$, α-Fe_2O_3 and metallic Fe. The mixture was heated at 900 °C in a sealed evacuated ($\sim 10^{-5}$ Torr) quartz tube for 5 h [11].

The x-ray diffraction pattern at RT was taken in the Bragg–Brentano geometry (from 15° to 80° with a step of 0.03°) with Cu Kα radiation using a graphite crystal monochromator (Siemens D500). The Rietveld profile analysis [12] using space group *Pbam* (No 55) revealed a single-phase material with no traces of any spurious phases (also confirmed from the Mössbauer spectra analysis). The refined values of the unit-cell parameters ($a = 9.4471(5)$ Å, $b = 12.2987(7)$ Å and $c = 3.0733(1)$ Å) were close to those reported in previous works [1,4]. The refined pattern is shown in figure 1(*b*).

Mössbauer spectra (MS) were collected in a transmission geometry in the temperature range 4.2–620 K, using a liquid-helium cryostat (Oxford Instruments), a closed-loop He system (Air Products and Chemicals) and a Mössbauer vacuum furnace. The temperature stability during all the measurements was better than ±0.5 K. The spectrometer was equipped with a ^{57}Co(Rh) source, kept at RT and calibrated with α-Fe. The isomer shift (IS) values are given relative to α-Fe at RT. Samples with different effective thicknesses were used to estimate saturation effects. During the sample holder preparation, special care was taken to avoid texture effects [11].

The magnetic susceptibility measurements were performed using a SQUID magnetometer (Quantum Design) in the temperature range 4.2–300 K. Four-probe resistivity measurements with and without a magnetic field were performed on a sintered bar of Fe_3BO_5 from 350 to 180 K (below which the extremely large resistance of the sample precluded accurate measurements).

3. Results and discussion

3.1. Magnetic susceptibility measurements

Magnetic susceptibility measurements in an applied magnetic field of 1 kOe in zero-field-cooling (ZFC) and in field-cooling (FC) modes are shown in figure 2. The plot of the inverse susceptibility ($1/\chi_g$) as a function of temperature (inset of figure 2) shows a deviation from linear dependence below 115 K. Above 115 K, the temperature dependence satisfies the Curie–Weiss law $\chi = C/(T - \Theta_p)$ with a rather large negative value of Θ_p and a Curie constant about 50% higher than that expected for the constituent free ions. These results imply prominent antiferromagnetic interactions and the existence of spin pair correlations in the paramagnetic state. So, it seems that the change in the slope of the $1/\chi_g$ versus T curve around 115 K marks the paramagnetic-to-antiferromagnetic transition ($T_N = 114$ K).

The ZFC and FC susceptibility curves are essentially the same above 75 K. At 75 K the ZFC susceptibility increases sharply, reaching a maximum at $T = 68$ K, and then decreases as the temperature decreases, reaching at around 40 K a value smaller than that for the paramagnetic state. The inset of figure 2 shows that the inverse susceptibility for the ZFC curve reaches a constant value at around 35 K. Below 70 K the ZFC and FC curves diverge, showing a hysteretic behaviour. The χ versus T variation between 40 and 70 K and the observed hysteresis in the remanent magnetization (from hysteresis loops that are not shown) are in agreement with previous work [4] showing that this material is a weak ferromagnet, suggesting ferrimagnetism or canted antiferromagnetism in this temperature region. Most probably the sharp peak below $T_w = 74$ K arises from two non-equivalent in magnitude antiferromagnetic sublattices.

The above described behaviour is nicely explained in the analysis of the MS (*vide infra*), which shows that between 75 and 115 K a magnetically ordered state including essentially the ferric and intermediate-valence ions coexists with a paramagnetic state involving Fe^{2+} ions.

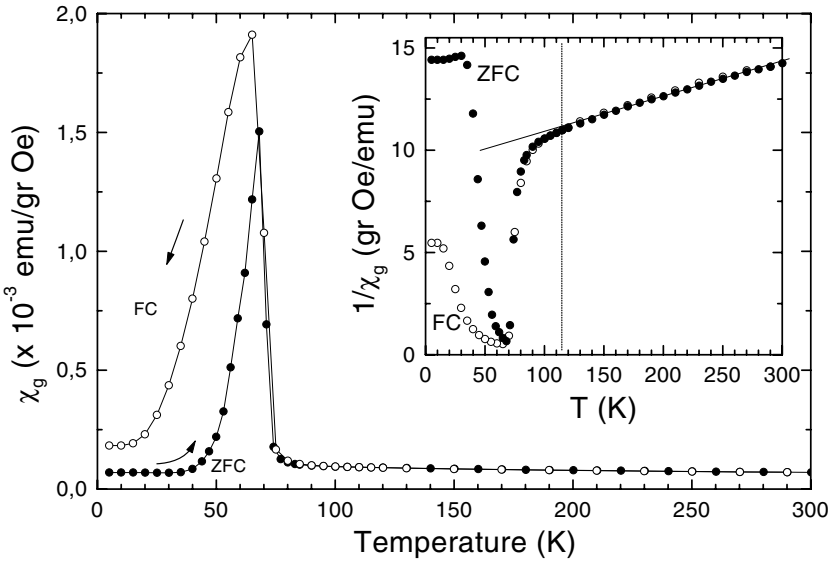

Figure 2. Magnetic susceptibility versus temperature in ZFC and FC modes for Fe_3BO_5 in applied magnetic field of 1 kOe. The filled symbols represent the ZFC curves and the open symbols are for the FC curves. Inset: the temperature variation of the inverse susceptibility ($1/\chi_g$). The vertical dashed line marks the antiferromagnetic transition ($T_N = 114$ K).

3.2. Resistance measurements

Figure 3 shows the temperature dependence of the resistance in a ln R versus $1/T$ plot that can be described by a thermally activated electron hopping law. The difference from previously published data on a single crystal is that in our sample the ln R versus $1/T$ curve is convex instead of being concave as in the single crystal [4]. This could be due to the anisotropy of the system [1]. In the bulk sample an average of the resistance over the three directions (or better over R_{ab} and R_c) is measured, whereas in the single crystal either R_{ab} or R_c can be measured. If the conduction is thermally activated, the resistance can vary as $R = A\exp(E_a/k_BT)$. On the ln R versus $1/T$ plot a gradual slope change occurs between 200 and 300 K and the high- and low-temperature activation energies are 0.50 and 0.21 eV, respectively. These might be associated with $Fe^{2+} \rightarrow Fe^{3+}$ and $3d^6 \rightarrow 3d^54s$ electron transfer, respectively, and is expected to influence the lineshape of the absorption lines in the MS [13]. Our MS (*vide infra*) support a picture with at least two temperature regions with different activation energies. Finally, we must note that in the present study the localization–delocalization transition T_{co} occurs around 250 K—that is, at a higher temperature than the one reported in the single-crystal study [4].

3.3. Mössbauer spectroscopy

Representative MS in the temperature range 4.2–620 K are shown in figures 4, 5, 7–9. For $T < 114$ K magnetically split MS are observed, while above this temperature the spectra are paramagnetic. In the temperature region $114 < T < 620$ K the spectra were fitted with paramagnetic doublets corresponding to charge-localized (Fe^{2+} or Fe^{3+}) as well as to charge-delocalized states. Charge-delocalized states are also observed at temperatures below 114 K where magnetic sextets or a combination of magnetic and paramagnetic components were used. In the following, due to the fact that the MS were analysed into several subcomponents, we use the letters D and S to denote the quadrupole doublets and magnetic sextets followed by the number of the particular component.

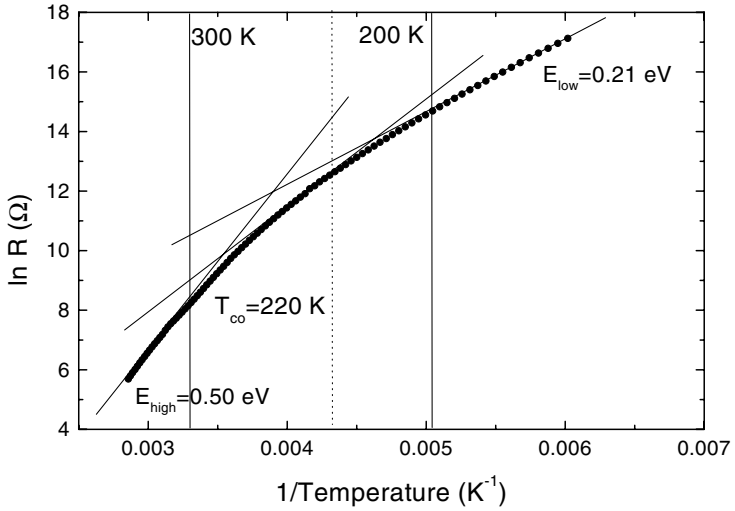

Figure 3. A ln R versus $1/T$ plot for Fe_3BO_5. The lines are used to denote the slope change as the temperature changes. The vertical lines denote the temperature range in which this slope change is observed. The vertical dashed line marks the delocalization–localization transition ($T_{co} \sim 220$ K) reported in [5].

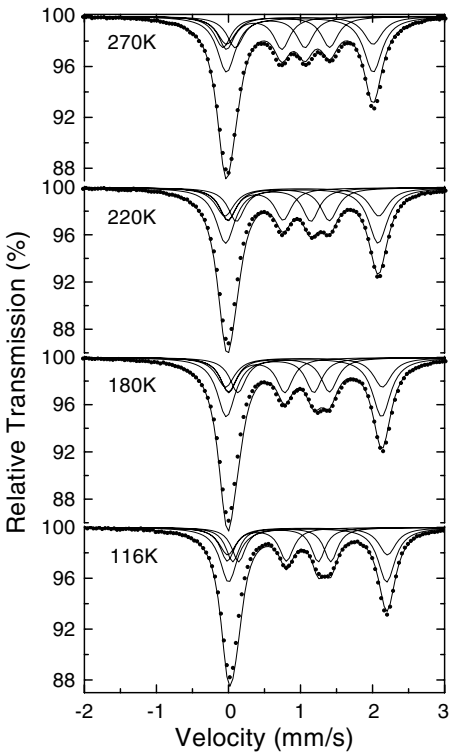

Figure 4. MS of Fe_3BO_5 recorded at temperatures between 116 and 270 K. The solid curves result from least-squares fits using Lorentzians (the parameters are shown in table 1).

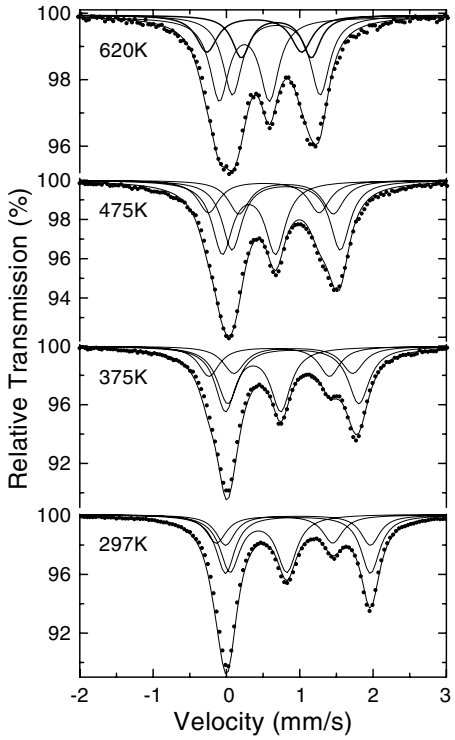

Figure 5. MS of Fe_3BO_5 recorded at temperatures between 297 and 620 K. The solid curves result from least-squares fits using Lorentzians (the parameters are shown in table 2).

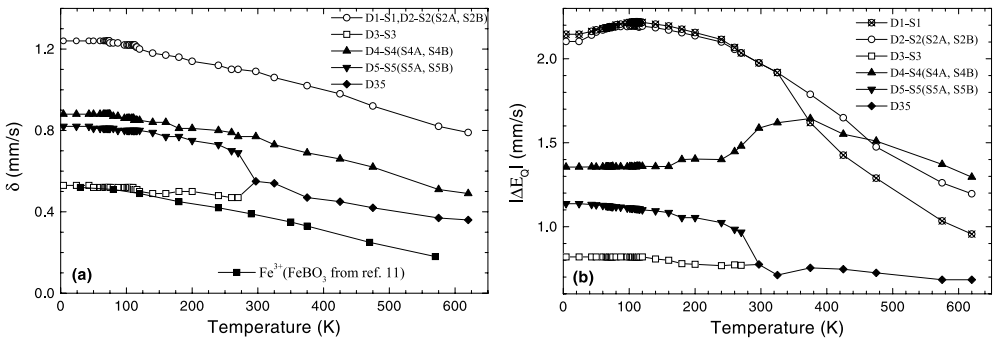

Figure 6. The temperature variation of (*a*) the isomer shift δ and (*b*) the quadrupole splitting ΔE_Q for the components presented in tables 1–5. The solid curves are guides to the eye.

3.3.1. Paramagnetic Mössbauer spectra. The MS recorded in the temperature region $114 < T < 270$ K (figure 4) show well resolved spectral lines, whereas for $T > 270$ K (figure 5) we observed broadened and more complex quadrupole-split MS.

In the first temperature range the profile of the MS suggests clearly that at least four doublets are necessary to fit the experimental data. However, the doublet that corresponds to the highest velocity requires a larger linewidth and area compared to the peaks in the middle of the spectrum, thereby suggesting two doublets instead of one. Indeed the use of

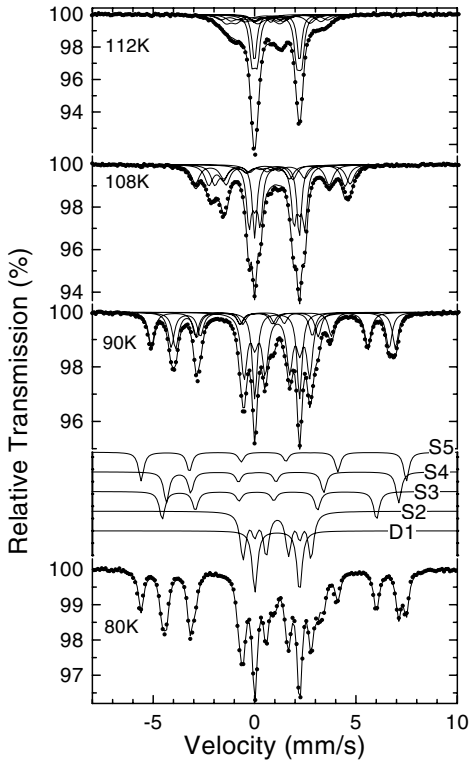

Figure 7. MS of Fe_3BO_5 at temperatures between T_N and T_w. Also shown are the components D1, S2, S3, S4 and S5 that were used to fit the spectra. The solid curves are least-squares fits as described in the text (the parameters are listed in table 3).

five doublets considerably improved the quality (χ^2) of the fit. Furthermore, these two sites are differentiated in the magnetic regime and at temperatures above 300 K (*vide infra*). The resulted Mössbauer parameters (MP) are listed in table 1. From their values and the fact that all iron ions are in octahedral oxygen coordination, it is clear that two of the doublets, D1 and D2, correspond to ferrous ions, and one, D3, cannot be readily interpreted as arising from pure Fe^{3+} in this temperature range [9, 14, 15]. Indeed for $T < 180$ K the IS values are indicative of an $Fe^{3+}O_6$ site and for $T > 180$ K the IS values are slightly larger than those expected for octahedral Fe^{3+}. Although this difference in the IS values is within the experimental error up to 220 K, it shows a clear tendency to increase with temperature and just above 270 K it increases abruptly. Therefore, doublet D3 can be assigned to a pure Fe^{3+} ion for $T < 180$ K and to a ferric-like 'Fe^{3+}' ion for $T > 180$ K [9, 14, 15]. The doublets D4 and D5 clearly have IS values very close to the average value for high-spin ferric and ferrous ions in octahedral oxygen coordination [9, 14, 15]. Thus, these two doublets can be assigned to iron ions with oxidation states very close to $Fe^{2.5+}$, which occur when the excess electron of Fe^{2+} is shared equally between one Fe^{2+} and one Fe^{3+} ion in the above environment. Also, from table 1, it can be seen that the delocalized states D4 and D5 have clearly distinct IS and quadrupole splitting (QS) values below 270 K indicating that the corresponding ions are in different valence states. The ions assigned to D5 have oxidation states higher than that of the ions assigned to the D4 component and both are very close to 2.5+. In order to distinguish the D4 and D5 ions from the D3 ions we denote these $Fe^{2.5+}$-like valence states by '$Fe^{2.5+}$'.

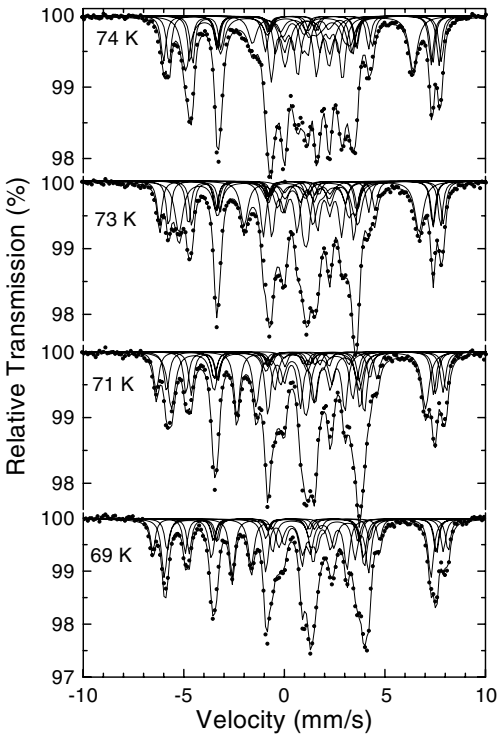

Figure 8. MS of Fe_3BO_5 that follow the development of the ferrimagnetic ordering at temperatures between 69 and 74 K. The solid curves are least-squares fits using Lorentzians (the parameters are shown in table 4).

Furthermore, table 1 shows that for $T > 180$ K the three intermediate-valence states assigned to doublets D3, D4, D5 have not only distinct IS and QS values but also their temperature dependencies are interrelated in a systematic and consistent way up to 270 K, where some major changes are observed (figure 6). Therefore these three iron sites should be neighbouring and from the sum of their IS values we can conclude that components D3, D4 and D5 can be assigned to three different iron ions forming a mixed-valence triad Fe^{3+}–Fe^{2+}–Fe^{3+}, where the excess electron of Fe^{2+} is partially delocalized among the three iron sites. Hence, we can conclude at this point that for $T < 180$ K the excess electron of the Fe^{2+} is partially delocalized between the two iron sites of the triad, leaving a trivalent ion at the third site, whereas for $T > 180$ K it is partially delocalized among the three available sites of the triad. It is interesting to note here that the ions assigned to doublet D4 keep their valence state unchanged up to 270 K, but these of D3 and D5 show a tendency to converge to the same valence state as the temperature is increased in the range $180 < T < 270$ K. We should also mention that we used only the IS values (and not the QS) as indicators of the oxidation state of the iron ions, because a direct comparison of the QS values of the intermediate-valence states with those of the localized states can be misleading, since the QS values are sensitive to additional factors other than the oxidation state of the ion (charge symmetry, anisotropic covalency, spin–orbit coupling).

The crystal structure of Fe_3BO_5 comprises four non-equivalent Fe sites [1]: Fe1 and Fe4 for Fe^{2+} and Fe2, Fe3 for the intermediate-valence Fe ions. In fact, the Fe1 and Fe4 divalent sites are located in a different plane ($z = 0$) from the Fe2 and Fe3 sites ($z = 1/2$). The latter

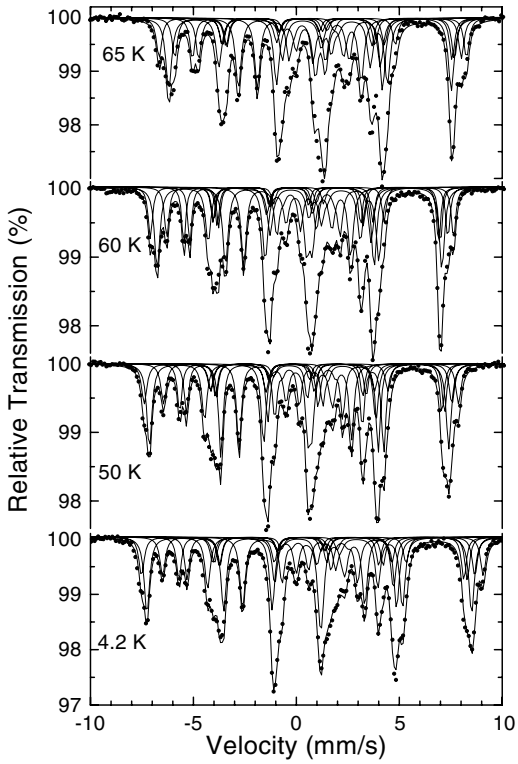

Figure 9. MS of Fe_3BO_5 at temperatures between 4.2 and 65 K. The solid curves are least-squares fits using Lorentzians (the parameters are shown in table 5).

form triads Fe3–Fe2–Fe3 (3–2–3) in which the iron ions are very close ($d_{23} = 2.787$ Å) and so the d–d overlap in the ab-plane is rather strong. As for the divalent sites, the corresponding distances are just at the limit of direct d–d overlap (d_{11} or d_{44} is just the lattice parameter c) or above this limit ($d_{14} = 3.374$ Å).

So, the assignment of the Mössbauer components for $T > 180$ K is the following. D1 corresponds to Fe^{2+} in site Fe1 and D2 to Fe^{2+} in site Fe4. Components D3, D4 and D5 originate from intermediate-valence ions within the 3–2–3 triads. Notably, even though the crystal structure of this phase has four non-equivalent octahedral sites, the Mössbauer analysis requires five distinct doublets. This can be explained by the existence of delocalized sites. As regards the resulting areas of the observed components, their ratio D1(Fe^{2+}):D2(Fe^{2+}):D3('Fe^{3+}'):D4('$Fe^{2.5+}$'):D5('$Fe^{2.5+}$') is equal to 1:2:1:1:1. If we multiply this ratio by 2, we find 2:4:2:2:2 and thus we can reproduce the 12 iron ions present in the ludwigite unit cell. So, assuming equal Debye–Waller factors for all iron sites, it turns out that $Fe^{2+}[D1 + D2 + (D3 + D4 + D5)/3]:Fe^{3+}[(2/3)(D3 + D4 + D5)] = 8:4$, which agrees exactly with the stoichiometry.

Above 270 K the profile of the spectra changes (figure 5) and four doublets are adequate for fitting the data (see table 2). More specifically we used D1, D2 and D4 with hyperfine parameters that are just a continuation from the temperature region below 270 K, together with a fourth doublet D35 that has IS and QS in the intermediate region between those of D3 and D5 and a spectral area equal to the sum of the areas of D3 and D5. Doublets D3 and D5 converge at 297 K into D35 with $\delta = 0.55$ mm s^{-1} which implies an intermediate-valence state for Fe.

Table 1. Experimental values of the isomer shift δ, the half-linewidth $\Gamma/2$ and the QS values ΔE_Q in mm s^{-1} as obtained from least-squares fits of the MS of Fe_3BO_5 between 116 and 270 K. Typical errors for the hyperfine parameters are ± 0.01 mm s^{-1} and for the site occupancies $\pm 3\%$.

T (K)	Component: Site:	D1 Fe^{2+}	D2 Fe^{2+}	D3 Fe^{3+}	D4 '$Fe^{2.5+}$'	D5 '$Fe^{2.5+}$'
116	δ	1.21	1.21	0.51	0.85	0.80
	ΔE_Q	2.22	2.19	0.82	1.36	1.11
	$\Gamma/2$	0.14	0.14	0.12	0.12	0.12
	Area (%)	17	33	17	16	17
180	δ	1.16	1.16	0.50	0.81	0.77
	ΔE_Q	2.18	2.16	0.78	1.40	1.05
	$\Gamma/2$	0.15	0.15	0.14	0.14	0.14
	Area (%)	16	33	17	17	17
220	δ	1.13	1.13	0.49	0.81	0.74
	ΔE_Q	2.14	2.12	0.77	1.41	1.03
	$\Gamma/2$	0.16	0.16	0.14	0.14	0.14
	Area (%)	16	33	17	17	17
270	δ	1.10	1.10	0.47	0.77	0.69
	ΔE_Q	2.03	2.04	0.77	1.48	0.97
	$\Gamma/2$	0.16	0.16	0.13	0.14	0.14
	Area (%)	16	33	17	17	17

Table 2. Experimental values of the isomer shift δ, the half-linewidth $\Gamma/2$ and the QS values ΔE_Q in mm s^{-1} as obtained from least-squares fits of the MS of Fe_3BO_5 between 297 and 620 K. Typical errors for the hyperfine parameters are ± 0.01 mm s^{-1} and for the site occupancies $\pm 3\%$.

T (K)	Component: Site:	D1 Fe^{2+}	D2 Fe^{2+}	D35 $Fe^{2.75+}$	D4 '$Fe^{2.5+}$'
297	δ	1.09	1.09	0.55	0.77
	ΔE_Q	1.98	1.98	0.78	1.59
	$\Gamma/2$	0.16	0.16	0.16	0.16
	Area (%)	17	33	33	17
375	δ	1.02	1.02	0.47	0.69
	ΔE_Q	1.62	1.79	0.76	1.64
	$\Gamma/2$	0.18	0.18	0.16	0.17
	Area (%)	16	33	34	17
475	δ	0.92	0.92	0.42	0.62
	ΔE_Q	1.29	1.48	0.73	1.51
	$\Gamma/2$	0.17	0.16	0.17	0.18
	Area (%)	17	33	34	16
620	δ	0.78	0.78	0.36	0.49
	ΔE_Q	0.97	1.19	0.68	1.28
	$\Gamma/2$	0.15	0.16	0.16	0.17
	Area (%)	17	33	33	17

This should correspond to a delocalized state within the 3–2–3 triad with a valence of +2.75: the extra half of a d electron which was residing in one site of the pair '$Fe^{+2.5}$'–Fe^{3+} for $T < 180$ K is now shared equally by these sites. Thus, above RT we do not observe three intermediate-valence ions since two of them undergo a localization–delocalization transition which starts at

180 K and is completed around 280 K. The region of this transition is also confirmed by the resistance measurements on our powder samples as well as on a single-crystal sample [4]. In the case of Fe_2BO_4 a charge-ordering transition is observed at $T_{co} \sim 320$ K [8, 9, 15] and is accompanied by a lattice distortion. Comparing the two cases, we see that the thermal evolution of the Mössbauer spectra around T_{co} is completely different. In the present system we observe a rather gradual change from a partially to a fully delocalized state, while in Fe_2BO_4 [9, 15] the system passed from a region where both localized and delocalized states were present. This can be explained by assuming that in Fe_2BO_4 the electrons localize due to their electrostatic repulsion in Wigner nanocrystals, whereas in Fe_3BO_5 a Wigner glass is formed instead [5]. The formation of this glass phase should be inherently connected to the preferential occupancy of the four non-equivalent octahedral sites by divalent and trivalent Fe ions.

Finally, it is useful to discuss some issues regarding the temperature variation of the hyperfine parameters of the various components. The isomer shift temperature variation up to 425 K (figure 6(*a*)) is the expected one for the ferrous ions of D1, D2 and for '$Fe^{2.5+}$' of D4 (with respect to the second-order Doppler shift). D3 and D5 follow a similar temperature behaviour in the temperature range 114–180 K: above 180 K they show a tendency to converge and above 300 K the charge-localization–delocalization transition leads to one component, D35, which has the expected temperature variation up to 425 K. Above 425 K the components D1, D2, D4 and D35 show a tendency to converge to the same valence state, indicating that charge delocalization is starting between them. In the temperature interval $114 < T < 270$ K the temperature variation of the QS (figure 6(*b*)) is the one expected for octahedrally coordinated Fe^{2+}, 'Fe^{3+}' and '$Fe^{2.5+}$' ions. Around 180 K, the QS values of components D4 and D5 show a rather small change and then around 250 K a gradual change is observed, that is completed at 300 K. Such changes can be associated with distortions in the iron site symmetry and thus with a crystal structure transition. It is interesting to note that at 180 K a localization–delocalization transition is started and we may assume that these two phenomena are related to each other. However, such a case is ruled out by the x-ray studies where no change was observed in the crystalline structure between RT and 93 K [4]. Thus, most probably, these changes in the QS values are due to rearrangement of the electronic charge inside the pair Fe^{+3}–'$Fe^{+2.5}$' within the 3–2–3 triad. In summary, the Fe^{2+} doublets D1 and D2 correspond to the Fe1 and Fe4 sites, respectively, and the intermediate-valence doublets D3, D4 and D5 to the Fe2 and Fe3 sites.

3.3.2. Magnetic Mössbauer spectra. Representative magnetic spectra are shown in figures 7–9. These spectra, according to their profile, define two temperature regions: one from 114 down to 75 K and the second between 75 and 4.2 K.

For $75 < T < 114$ K magnetic and paramagnetic components coexist (figure 7). Starting the analysis from the 80 K spectrum, where the absorption lines are sharp and well resolved, we note some specific characteristics of this multicomponent spectrum. First, there are two sharp lines of equal intensities located at velocities close to 0 and to 2 mm s^{-1}. Comparing with the spectra in the paramagnetic region, it becomes immediately clear that these two lines belong to an Fe^{2+} doublet. Second, there is a significant spectral area surrounding symmetrically each line of this doublet which most probably can be attributed to magnetically split divalent iron with a small magnetic hyperfine field H_{eff}. Third, the three rightmost absorption lines are very sharp, have almost equal intensities and are closely positioned. These features indicate that these three lines are the rightmost lines of three individual sextets. Now, considering that the separation between the lines 5 and 6 of a sextet is related to the QS value and that in the paramagnetic region the delocalized doublets have a larger QS value compared to the ferric doublet, we speculate that the outer two lines belong to magnetic sextets that correspond to $Fe^{2.5+}$. So, the remaining line located around 6 mm s^{-1} is the sixth line of an Fe^{3+} sextet.

Taking into consideration the above discussion, we fitted the spectrum at 80 K, by employing one Fe^{2+} doublet and four Zeeman-split (sextets) components with Lorentzian lineshape. The initial values for IS and QS parameters were deduced from the results for the paramagnetic region (with the appropriate corrections for the isomer shift due to second-order Doppler shift).

Adopting this fitting scheme for all spectra between 80 and 108 K, we got satisfactory χ^2-fits and consistent hyperfine parameters. Representative MS at 80, 90 and 108 K are shown in figure 7 and the corresponding parameters are listed in table 3. Comparing the hyperfine parameters shown in tables 1 and 3, we can conclude that the magnetic components in this temperature region can be directly assigned to the paramagnetic components observed above 114 K corresponding to two Fe^{2+}, one Fe^{3+} and two '$Fe^{+2.5}$' ions.

Between 110 and 114 K a paramagnetic central feature appears which dominates the spectrum as we approach the transition temperature 114 K. This is not a typical behaviour for an isotropic magnetically ordered system, where the MS below the transition temperature consist only of sextets with narrow Lorentzian lines. This temperature evolution of the MS as we approach T_c has been observed in a similar oxyborate system [9, 15] and in several other studies [16–23]. The spectra in this temperature range were fitted using a combination of a paramagnetic plus a magnetic part for each site. A representative result of a fit at $T = 112$ K is shown in figure 7. From the above analysis it is clear that in the temperature range 108–75 K, all iron ions order magnetically apart from those assigned to the component D1 which are frustrated and order only when the temperature is lowered below 75 K.

In the temperature range $4.2 < T < 75$ K (figures 8 and 9) the MS appear much more complicated than those observed above 75 K. These spectra comprise more absorption lines and the five-component model used above 75 K cannot reproduce them. On cooling below 75 K the quadrupole doublet D1 gradually becomes magnetic and this process is completed at 69 K. Below this temperature the shape of the MS is typical for a multicomponent Zeeman-split spectrum.

Comparison of the spectra at 74 and 80 K shows that the leftmost line of component S5, located around -6 mm s^{-1} (see the bottom spectrum of figure 7), becomes less intense and broadens at 74 K, although the area remains the same. A careful examination of the lineshape suggests that the broadening should be the result of two overlapping Lorentzian lines with equal areas. In contrast, in the same spectrum, the rightmost line of component S3 ($\sim$6 mm s^{-1}) also broadens and loses intensity but it can be fitted with just one broad Lorentzian line. Examining carefully the rest of the absorption lines of the spectra below 74 K, we came to the conclusion that at 74 K all components (except S1 and S3) should be separated into two components with the same IS, QS and asymmetry parameter η, but with different values for H_{eff} and the polar angles θ and ϕ. Thus, for the analysis of the spectra below 75 K, we employed eight sextets. For the temperature range 69–74 K we had to add two extra components, the paramagnetic D1 which becomes gradually magnetic and the sextet S2 which gradually splits into two components. It should also be noticed that in order to examine in detail and consistently the evolution of every single component between 69 and 74 K, we recorded MS every 1 K for this interval where major changes occur and every 5 K for temperatures below 70 K. With this fitting model we were able to simulate the experimental data very successfully for such a multi-parameter system (see figures 8 and 9) and to obtain consistent MP (tables 4 and 5).

The temperature variation of the magnetic hyperfine fields H_{eff} of the various components is shown in figure 10. There are clearly two regions, defined by two magnetic transitions: the first, an antiferromagnetic transition concerning the ferric, intermediate-valence and some of the Fe^{2+} ions, occurs at $T_N = 114$ K and the second, a ferrimagnetic transition, occurs at $T_w = 74$ K where all Fe^{2+} become magnetically ordered.

Table 3. Experimental values of the isomer shift δ, the half-linewidth $\Gamma/2$ and the QS values ΔE_Q in mm s^{-1}, the hyperfine magnetic field H_{eff} in kG and the angles θ and ϕ in degrees as obtained from least-squares fits of the MS of Fe_3BO_5 between T_N and 80 K. η is the asymmetry parameter of the EFG tensor and θ and ϕ are the polar angles of the hyperfine magnetic field in the EFG tensor. Typical errors are ± 0.01 mm s^{-1} for δ, $\Gamma/2$ and ΔE_Q, ± 3 kG for H_{eff}, ± 0.1 for η, $\pm 5^\circ$ for θ, $\pm 10^\circ$ for ϕ and $\pm 3\%$ for the site occupancies. We should note that the errors on η, θ and ϕ are considerably enhanced close to the magnetic transition temperatures.

T (K)	Component: Site:	D1 Fe^{2+}	S2 Fe^{2+}	S3 Fe^{3+}	S4 '$Fe^{2.5+}$'	S5 '$Fe^{2.5+}$'	D2 Fe^{2+}	D3 Fe^{3+}	D4 '$Fe^{2.5+}$'	D5 '$Fe^{2.5+}$'
112	δ	1.22	1.22	0.50	0.85	0.80	1.22	0.50	0.85	0.80
	ΔE_Q	2.22	2.20	0.82	1.36	1.11	2.22	0.82	1.36	1.11
	$\Gamma/2$	0.14	0.14	0.29	0.29	0.30	0.20	0.21	0.36	0.36
	H_{eff}		12	123	119	152				
	η		0.3	0	0.2	0.3				
	θ		54	21	20	27				
	ϕ		75	0	63	90				
	Area (%)	17	29	13	11	8	4	4	6	8
108	δ	1.22	1.22	0.51	0.86	0.80				
	ΔE_Q	2.20	2.20	0.82	1.36	1.11				
	$\Gamma/2$	0.13	0.14	0.24	0.22	0.25				
	H_{eff}		23	181	191	228				
	η		0.3	0	0.2	0.3				
	θ		54	21	15	36				
	ϕ		75	0	62	91				
	Area (%)	17	33	17	16	17				
90	δ	1.23	1.23	0.51	0.87	0.80				
	ΔE_Q	2.21	2.19	0.82	1.36	1.12				
	$\Gamma/2$	0.15	0.18	0.18	0.18	0.18				
	H_{eff}		42	299	325	368				
	η		0.3	0	0.2	0.3				
	θ		54	21	12	36				
	ϕ		75	0	60	90				
	Area (%)	16	34	17	17	16				
80	δ	1.23	1.23	0.52	0.87	0.81				
	ΔE_Q	2.20	2.19	0.82	1.36	1.12				
	$\Gamma/2$	0.15	0.17	0.16	0.15	0.15				
	H_{eff}		46	327	354	401				
	η		0.3	0	0.2	0.3				
	θ		53	22	11	35				
	ϕ		78	0	61	90				
	Area (%)	17	33	16	18	16				

The hyperfine fields of components S3, S4 and S5 (sites originating from trivalent states and from intermediate-valence states within the 3–2–3 triads) rise fast below 114 K and seem to follow a mean-field variation with temperature above 74 K, typical for an ordered system. The Fe^{2+} ions of site S1, that is the two Fe1 ions, are not ordered until 74 K is reached. The observed zero hyperfine-field value of the S1 component may be due to the frustration between the antiferromagnetically (AFM) and ferromagnetically (FM) ordered chains. At this point it is useful to consider the magnetic structure of Fe_3BO_5 [2]. It comprises ferromagnetic chains of Fe^{2+} with a ferromagnetic interchain coupling and antiferromagnetic chains of predominantly Fe^{3+} character with antiferromagnetic interchain coupling. The hyperfine field for the four Fe4

Table 4. Experimental values of the isomer shift δ, the half-linewidth $\Gamma/2$ and the QS values ΔE_Q in mm s^{-1}, the hyperfine magnetic field H_{eff} in kG and the angles θ and ϕ in degrees as obtained from least-squares fits of the MS of Fe_3BO_5 between T_w and 69 K. η is the asymmetry parameter of the EFG tensor and θ and ϕ are the polar angles of the hyperfine magnetic field in the EFG tensor. Typical errors are ± 0.01 mm s^{-1} for δ, $\Gamma/2$ and ΔE_Q, ± 3 kG for H_{eff}, ± 0.1 for η, $\pm 5^\circ$ for θ, $\pm 10^\circ$ for ϕ and $\pm 3\%$ for the site occupancies. We should note that the errors on η, θ and ϕ are considerably enhanced close to the magnetic transition temperatures.

T (K)	Component: Site:	S1 Fe^{2+}	S2A Fe^{2+}	S2B Fe^{2+}	S3 Fe^{3+}	S4A '$Fe^{2.5+}$'	S4B '$Fe^{2.5+}$'	S5A '$Fe^{2.5+}$'	S5B '$Fe^{2.5+}$'	D1 Fe^{2+}	S2 Fe^{2+}
74	δ	1.23	1.23	1.23	0.52	0.87	0.87	0.81	0.81	1.23	1.23
	ΔE_Q	2.19	2.19	2.19	0.82	1.36	1.36	1.12	1.12	2.19	2.19
	$\Gamma/2$	0.16	0.24	0.16	0.25	0.14	0.14	0.15	0.14	0.26	0.18
	H_{eff}	38	118	84	350	369	370	424	412		54
	η	0.5	0.3	0.3	0	0.2	0.2	0.3	0.3		0.3
	θ	50	90	44	19	19	9	39	33		52
	ϕ	54	34	34	0	40	1	57	60		57
	Area (%)	9	9	9	17	8	8	8	8	8	16
73	δ	1.24	1.24	1.24	0.52	0.88	0.88	0.81	0.81	1.24	1.24
	ΔE_Q	2.19	2.19	2.19	0.82	1.36	1.36	1.12	1.12	2.19	2.19
	$\Gamma/2$	0.16	0.22	0.16	0.25	0.14	0.14	0.15	0.14	0.26	0.18
	H_{eff}	52	146	91	369	374	372	433	415		65
	η	0.5	0.3	0.3	0	0.2	0.2	0.3	0.3		0.3
	θ	50	85	47	22	19	9	43	31		53
	ϕ	54	34	34	0	40	0	57	60		57
	Area (%)	14	14	14	17	8	8	8	8	3	6
71	δ	1.24	1.24	1.24	0.52	0.87	0.87	0.81	0.81	1.24	1.24
	ΔE_Q	2.19	2.19	2.19	0.82	1.36	1.36	1.12	1.12	2.19	2.19
	$\Gamma/2$	0.16	0.17	0.18	0.22	0.15	0.15	0.16	0.16	0.15	0.15
	H_{eff}	66	170	116	391	382	373	443	423		78
	η	0.5	0.3	0.3	0	0.2	0.2	0.3	0.3		0.3
	θ	58	85	51	25	18	10	43	30		53
	ϕ	54	34	34	0	40	1	57	60		57
	Area (%)	15	15	16	17	8	8	8	8	2	3
69	δ	1.24	1.24	1.24	0.52	0.88	0.88	0.81	0.81		
	ΔE_Q	2.18	2.18	2.18	0.82	1.36	1.36	1.12	1.12		
	$\Gamma/2$	0.16	0.16	0.18	0.16	0.14	0.14	0.15	0.15		
	H_{eff}	74	186	133	410	385	380	451	422		
	η	0.5	0.3	0.3	0	0.2	0.2	0.3	0.3		
	θ	58	84	53	30	18	9	46	29		
	ϕ	54	34	34	0	40	0	57	60		
	Area (%)	17	17	17	17	8	8	8	8		

ions neighbouring with the Fe1 ions is small above 74 K and increases to 100 kG at $T = 74$ K, implying the existence of frustration and/or imperfect ordering. At 74 K, component S2 separates in two components (S2A and S2B) with magnetic hyperfine fields that differ by $\sim$50 kG at 4.2 K. The sudden changes in H_{eff} for components S2 and S3 at $T_w = 74$ K could indicate that the sublattice of the frustrated spins is coupled to these magnetically ordered sublattices. Similar effects were observed in several other studies [24–26]. The two separated components of S4 and S5 show a smaller difference in their hyperfine fields with respect to S2 (a maximum of $\sim$14 kG at 4.2 K for S4 and a maximum of $\sim$40 kG at 4.2 K for S5). Also, they exhibit only a slight change as a result of the ordering of the S1 (Fe^{2+}) ions at T_w.

Table 5. Experimental values of the isomer shift δ, the half-linewidth $\Gamma/2$ and the QS values ΔE_Q in mm s^{-1}, the hyperfine magnetic field H_{eff} in kG and the angles θ and ϕ in degrees as obtained from least-squares fits of the MS of Fe_3BO_5 between 4.2 and 65 K. η is the asymmetry parameter of the EFG tensor and θ and ϕ are the polar angles of the hyperfine magnetic field in the EFG tensor. Typical errors are ± 0.01 mm s^{-1} for δ, $\Gamma/2$ and ΔE_Q, ± 3 kG for H_{eff}, ± 0.1 for η, $\pm 5^\circ$ for θ, $\pm 10^\circ$ for ϕ and $\pm 3\%$ for the site occupancies.

T (K)	Component: / Site:	S1 Fe^{2+}	S2A Fe^{2+}	S2B Fe^{2+}	S3 Fe^{3+}	S4A '$Fe^{2.5+}$'	S4B '$Fe^{2.5+}$'	S5A '$Fe^{2.5+}$'	S5B '$Fe^{2.5+}$'
65	δ	1.24	1.24	1.24	0.52	0.88	0.88	0.81	0.81
	ΔE_Q	2.18	2.18	2.18	0.82	1.36	1.36	1.12	1.12
	$\Gamma/2$	0.16	0.17	0.15	0.17	0.14	0.14	0.15	0.15
	H_{eff}	77	201	150	424	392	381	458	429
	η	0.5	0.3	0.3	0	0.2	0.2	0.3	0.3
	θ	58	80	55	30	19	9	47	27
	ϕ	55	34	36	0	41	2	57	60
	Area (%)	17	17	17	17	8	8	8	8
60	δ	1.24	1.24	1.24	0.52	0.88	0.88	0.81	0.81
	ΔE_Q	2.17	2.18	2.18	0.82	1.36	1.36	1.13	1.13
	$\Gamma/2$	0.16	0.17	0.15	0.16	0.11	0.11	0.13	0.13
	H_{eff}	87	221	170	449	403	393	475	442
	η	0.5	0.3	0.3	0	0.2	0.2	0.3	0.3
	θ	57	81	56	30	20	9	47	27
	ϕ	54	34	34	0	40	0	57	60
	Area (%)	17	17	17	17	8	8	8	8
50	δ	1.24	1.24	1.24	0.52	0.88	0.88	0.81	0.81
	ΔE_Q	2.16	2.17	2.17	0.82	1.36	1.36	1.13	1.13
	$\Gamma/2$	0.15	0.13	0.14	0.15	0.13	0.13	0.16	0.16
	H_{eff}	92	237	187	472	416	404	493	453
	η	0.5	0.3	0.3	0	0.2	0.2	0.3	0.3
	θ	59	79	57	33	20	9	49	25
	ϕ	54	34	35	0	43	1	57	64
	Area (%)	17	17	17	17	8	8	8	8
4.2	δ	1.24	1.24	1.24	0.53	0.88	0.88	0.82	0.81
	ΔE_Q	2.10	2.15	2.15	0.82	1.36	1.36	1.14	1.14
	$\Gamma/2$	0.15	0.16	0.16	0.16	0.14	0.14	0.15	0.15
	H_{eff}	95	249	201	488	431	417	511	468
	η	0.5	0.3	0.3	0	0.2	0.2	0.3	0.3
	θ	60	78	57	34	21	9	48	26
	ϕ	54	35	35	0	42	2	56	62
	Area (%)	17	17	17	17	8	8	8	8

The pronounced increase in the H_{eff} of component S3 could indicate a direct interaction with the iron ions corresponding to the S1 component. Note that the ferrimagnetic transition is hardly detectable in the H_{eff} versus T variation of the S4 and S5 components, apart from the above-mentioned separation into two components.

The observation of two transitions, with the second concerning only some of the Fe^{2+} ions, is reminiscent of so-called 'idle-spin' behaviour [26]. The delayed ordering of the divalent Fe1 ions can result from their specific topology in the Fe_3BO_5 unit cell. Indeed, in the present case the Fe1 ions are located at the centre of a tetragonal spin configuration consisting of the Fe3 ions. The latter ions form antiferromagnetic chains along the c-axis. Thus, the spins of the Fe1 ions are frustrated in an effort to order due to the magnetic interactions with

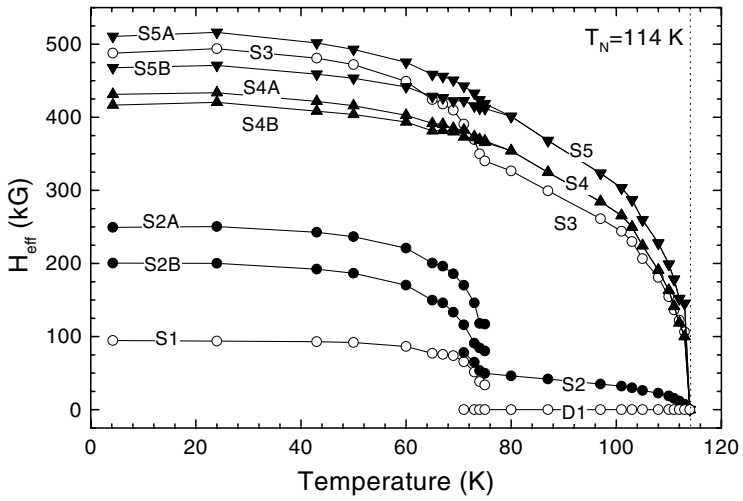

Figure 10. The temperature variation of the effective hyperfine field (H_{eff}) for the components presented in tables 3–5. The solid curves are guides to the eye. The vertical dashed line marks the antiferromagnetic transition ($T_N = 114$ K).

their neighbours. Neutron diffraction experiments in the temperature range between 4.2 and 114 K would be extremely useful for showing the variation of the magnetic structure in this temperature range.

4. Conclusions

We report on dc magnetometry, resistivity and Mössbauer spectroscopy measurements on Fe_3BO_5 in a wide temperature range from 4.2 to 620 K. The MS were consistently interpreted throughout the whole temperature range. Mössbauer spectroscopy has shown the paramagnetic-to-antiferromagnetic transition at $T_N = 114$ K, as well as the transition to a weak ferromagnetic state at $T_w = 74$ K. Between 75 and 114 K the Fe^{2+} ions in the basal plane (crystallographic site Fe1) remain paramagnetic (doublet D1). This unusual magnetic behaviour known as 'idle-spin behaviour' can be explained by the fact that, along the c-axis, the Fe1 ions are located at the centre of a rectangle with Fe3 ions on its corners. At T_w the effective hyperfine fields of components S1 and S2 which correspond to the Fe sites on the basal planes (Fe1 and Fe4, respectively) increase dramatically. The effective hyperfine fields of components S3, S4 and S5 that correspond to the Fe sites within the $z = 1/2$ planes (Fe2 and Fe3) show a smaller change at T_w. The MS could only be fitted by considering that these components are separated into two with the same IS, QS and asymmetry parameter η, but with different values for H_{eff} and the polar angles θ and ϕ. The change recorded in the dc magnetization and Mössbauer data indicates that the magnetic structure of Fe_3BO_5 could change at 75 K, where the spin frustration gradually decreases. Most probably the onset of the magnetic ordering of the Fe1 ions creates differences in the exchange and super-exchange pathways on the same sublattice resulting in differences in the hyperfine fields and magnetization below T_w. The details of these magnetic transitions and the complete assignments of the Mössbauer magnetic components are still not resolved. Electron delocalization in the Fe3–Fe2–Fe3 triads between pairs of Fe^{2+} and Fe^{3+} ions was observed at all temperatures between 4.2 and 180 K and is found to coexist with localized ferric and ferrous (Fe1 and Fe4 crystallographic sites)

states. Above 180 K the delocalization in the 3–2–3 triads includes the rest of the Fe^{3+} ions. The resistivity data also provide evidence for the localization–delocalization transition. The important, but still not clear, features of these delocalized triads are the exact distribution of the iron oxidation states among the metal ions Fe3–Fe2–Fe3 and the dynamics of their electronic configurations across the temperature range 4.2–620 K. Finally, further Mössbauer studies and magnetic measurements in various applied magnetic fields accompanied by neutron powder diffraction measurements on the Fe_3BO_5 compound are under way, in order to clarify the above-mentioned unresolved issues.

Acknowledgments

We are grateful to Dr A Simopoulos for helpful discussions and a critical reading of the manuscript. Thanks are also due to Dr E Devlin for fruitful discussions and support in the measurements. We also thank a referee for bringing to our attention an observation concerning the temperature variation of the isomer shifts. Partial support of this work was provided by the PENED-1991 programme from the Greek GSRT and by the 'Georgiou Stayrou' Foundation through a scholarship to APD.

Note added in proof. During the editorial processing of this paper, a work by Mir *et al* [27] reported XRD measurements on a single crystal of Fe_3BO_5 and showed for the first time that at 283 K a structural transition occurs, resulting in five non-equivalent iron sites below 283 K, in complete agreement with our analysis with five non-equivalent iron sites for $T < 270$ K and with the temperature variation of the QS around RT.

References

[1] Swinnea J S and Steinfink H 1983 *Am. Mineral.* **68** 827
[2] Attfield J P, Clarke J F and Perkins D A 1992 *Physica* B **180+181** 581
[3] Douvalis A P, Papaefthymiou V, Bakas T and Moukarika A 1997 *Magnetic Hysteresis in Novel Magnetic Materials (NATO ASI Series vol 338)* ed G C Hadjipanayis (Dordrecht: Kluwer) p 761
[4] Guimaraes R B, Mir M, Fernandes J C, Continentino M A, Borges H A, Cernicchiaro G, Fontes M B, Candela D R S and Baggio-Saitovich E 1999 *Phys. Rev.* B **60** 6617
[5] Fernandes J C, Guimaraes R B, Continentino M A, Ghivelder L and Freitas R S 2000 *Phys. Rev.* B **61** R850
[6] Bertaut E F 1950 *Acta Crystallogr.* **3** 473
[7] Takeuchi Y, Watanabe T and Ito T 1950 *Acta Crystallogr.* **3** 98
[8] Attfield J P, Bell A T M, Rodriguez-Martinez L M, Greneche J M, Cernik R J, Clarke J F and Perkins D A 1998 *Nature* **396** 655
Attfield J P, Bell A T M, Rodriguez-Martinez L M, Greneche J M, Retoux R, Leblanc M, Cernik R J, Clarke J F and Perkins D A 1999 *J. Mater. Chem.* **9** 205
[9] Douvalis A P, Papaefthymiou V, Moukarika A, Bakas T and Kallias G 2000 *J. Phys.: Condens. Matter* **12** 177
[10] Li Z, Stevens J G, Zhang Y and Zeng Y 1994 *Hyperfine Interact.* **83** 489
[11] Douvalis A P 2000 *PhD Thesis* University of Ioannina
[12] Rietveld H M 1969 *J. Appl. Crystallogr.* **2** 65
[13] Coey J M D, Allan J, Xuemin K, Van Dang N and Ghose S 1984 *J. Appl. Phys.* **55** 1963
[14] Coey J M D 1984 *Mössbauer Spectroscopy Applied to Inorganic Chemistry* vol 1, ed G J Long (New York: Plenum) p 450
[15] Douvalis A P, Papaefthymiou V, Moukarika A and Bakas T 2000 *Hyperfine Interact.* **126** 319
[16] Pissas M, Kallias G, Devlin E, Simopoulos A and Niarchos D 1997 *J. Appl. Phys.* **81** 5770
[17] Simopoulos A, Pissas M, Kallias G, Devlin E, Panagiotopoulos I, Moutis N, Niarchos D, Christides C and Sonntag R 1999 *Phys. Rev.* B **59** 1263
[18] Simopoulos A, Kallias G, Devlin E and Pissas M 2000 *Phys. Rev.* B **63** 054403
[19] Chechersky V, Nath A, Isaac I, Franck J P, Ghosh K, Ju H and Greene R L 1999 *Phys. Rev.* B **59** 497

[20] Ogale S B, Shreekala R, Bathe R, Date S K, Patil S I, Hannoyer B, Petit F and Marest G 1998 *Phys. Rev.* B **57** 7841
[21] Tkachuk A, Rogacki K, Brown D E, Dabrowski B, Fedro A J, Kimball C W, Pyles B, Xiong X, Rosenman D and Dunlap B D 1998 *Phys. Rev.* B **57** 8509
[22] Leung L K, Morrish A H and Evans B J 1976 *Phys. Rev.* B **13** 4069
[23] Morup S, Hendriksen P V and Linderoth S 1995 *Phys. Rev.* B **52** 287
[24] Leblanc M, Ferey G, Calage Y and de Pape R 1984 *J. Solid State Chem.* **53** 360
[25] Greneche J M 1988 *J. Magn. Magn. Mater.* **73** 115
[26] Ferey G 1991 *Mixed Valency Systems: Applications in Chemistry, Physics and Biology* ed K Prassides (Dordrecht: Kluwer) p 155
[27] Mir M, Guimaraes R B, Fernandes J C, Continentino M A, Doriguetto A C, Mascarenhas Y P, Ellena J, Castellano E E, Freitas R S and Ghivelder L 2001 *Phys. Rev. Lett.* **87** 147201